Combustion and Flame 161 (2014) 612–619

Contents lists available at ScienceDirect

Combustion and Flame

journal homepage: www.elsevier.com/locate/combustflame

The conversion mode of a porous carbon particle during oxidation and gasification

Nils Erland L. Haugen [a,*], Matthew B. Tilghman [b], Reginald E. Mitchell [b]

[a] SINTEF Energy Research, NO-7465 Trondheim, Norway
[b] Department of Mechanical Engineering, Stanford University, USA

ARTICLE INFO

Article history:
Received 5 June 2013
Received in revised form 17 September 2013
Accepted 17 September 2013
Available online 5 October 2013

Keywords:
Combustion
Porous particle
Char conversion mode

ABSTRACT

Studies have shown that both char particle diameter and apparent density vary during char conversion at high temperatures. To account for such variations, power-law expressions have been used to correlate $r_p/r_{p,0}$ and $\rho_p/\rho_{p,0}$ with $m_p/m_{p,0}$. The parameters in these relations are constants, thus this approach fails to account for variations in the functional relationship between mass, size, and apparent density as mass conversion proceeds. To overcome this limitation, a model for the mode of particle conversion has been developed that permits the variation in size and apparent density with mass loss to depend upon the Thiele modulus, which varies during char conversion. The rate with which the particle radius decreases is shown to be given by the ratio of the time derivative and the spatial derivative of the particle density at the surface of the particle. The model presented can be used to describe the mode of conversion of reactive porous particles in a range of different applications such as entrained flow gasifiers, pulverized coal burners and circulating fluidized bed combustors. There are no free tunable parameters in the model.

1. Introduction

In environments typical of pulverized coal-fired boilers and furnaces, char particles burn with variations in both size and apparent density. In order to reflect this phenomenon in char conversion models, power law relations have been used to correlate particle size and apparent density with char conversion [1,2]. In the approaches taken, the parameters in the relations are constants, thus the manner in which apparent density and diameter vary with mass loss during the initial stages of conversion is the same as that during the later stages. As particle mass is consumed due to the chemical reactions, pore diffusional resistances lessen as closed-off pores open and pores merge and coalesce, while the particle radius and the ambient conditions may also change. Thus, the functional relationships between extent of mass loss and particle size and apparent density are expected to change as mass conversion progresses.

In previous approaches to model the mode of conversion, the particle mass, diameter, and apparent density are assumed to be related via the following two relations (see for example Refs. [1–5]):

$$\frac{\rho_p}{\rho_{p,0}} = \left(\frac{m_p}{m_{p,0}}\right)^{\alpha}, \tag{1}$$

and

$$\frac{r_p}{r_{p,0}} = \left(\frac{m_p}{m_{p,0}}\right)^{\beta}. \tag{2}$$

In our proposed approach these expressions are rewritten in a piecewise form as:

$$\frac{\rho_p(t+\delta t)}{\rho_p(t)} = \left(\frac{m_p(t+\delta t)}{m_p(t)}\right)^{\alpha}, \tag{3}$$

and

$$\frac{r_p(t+\delta t)}{r_p(t)} = \left(\frac{m_p(t+\delta t)}{m_p(t)}\right)^{\beta}, \tag{4}$$

where ρ_p, r_p and m_p are the apparent density, radius and mass of the particle, respectively, t is the time and δt is a short time interval in which the power law assumption holds for values of α and β effective over the time interval. Furthermore, by assuming spherical particles, at any given time it follows that

$$\alpha(t) + 3\beta(t) = 1. \tag{5}$$

For $\alpha = 0$, particle conversion proceeds at constant density. This correspond to the zone III burning regime in which mass conversion occurs at high temperatures, rendering mass loss rates limited by the rates of reactant diffusion to the outer surface of the particle, and the particle reacts primarily at its periphery. Its apparent density is relatively unchanged and its diameter varies to the one-third power with mass loss. The specific surface area of the particle is

* Corresponding author.
E-mail addresses: nils.e.haugen@sintef.no, nils.e.haugen@gmail.com (N.E.L. Haugen).

0010-2180/$ - see front matter © 2013 The Combustion Institute. Published by Elsevier Inc. All rights reserved.
http://dx.doi.org/10.1016/j.combustflame.2013.09.012

Nomenclature

A_k	pre-exponential factor of reaction k
$A_{\text{int,eff}}$	effective internal surface area (m^2)
A_{ext}	external surface area (m^2)
$C(r,t)$	reactant concentration at particle radius r and time t (mol/m^3)
C_R	reactant concentration at particle periphery (mol/m^3)
D_{eff}	effective diffusivity inside the particle (m^2/s)
$dV(r,t)$	volume at time t of shell with radius r and thickness dr
E_k	activation energy of reaction k (MJ/kmol)
I	auxiliary variable as defined by Eq. (30) (s mol/m^2)
k	rate constant (1/s)
M_c	molar weight of carbon (kg/mol)
m_p	particle mass (kg)
$m(r,t)$	mass of shell inside particle at radius r, time t and with thickness dr (kg)
r_p	particle radius (m)
R	mass consumption rate per unit volume ($kg/s/m^3$)
S_{gc}	specific char surface area (m_2/kg)
t	time (s)
t'	dummy integration variable (s)
V_p	particle volume (m^3)
x	char conversion (–)
x_τ	char conversion when $t = \tau$ (–)

Greek symbols

α	exponent in $\rho_p - m_p$ relation (–)
β	exponent in $r_p - m_p$ relation (–)
δt	infinitesimal time (s)
η	effectiveness factor (–)
$\bar{\eta}$	mean effectiveness factor (–)
ν	stoichiometric coefficient (–)
ρ_p	apparent particle density (kg/m^3)
$\rho(r,t)$	apparent density at particle radius r and time t (kg/m^3)
ϕ	Thiele modulus (–)
σ_k	distribution width of activation energy for reaction k (MJ/kmol)

relatively unchanged in this conversion regime, due to reaction rates in the interior being nearly negligible. For $\alpha = 1$, particles conversion proceeds at constant diameter, which corresponds to the zone I burning regime. Here mass conversion occurs at low temperatures, rendering mass loss rates limited by chemical reaction rates, and the particle reacts more or less uniformly throughout its volume. The particle size is relatively unchanged and the apparent density varies proportionally with mass loss. The surface area per unit volume initially increases, reaching a maximum before decreasing with increasing extents of conversion. The surface area can be predicted using the grain and pore models that have been developed for such uniform burning (see for example, the random pore model of Bhatia and Perlmutter [6]). For $0 < \alpha < 1$, particles decrease in both size and apparent density, and this correspond to the zone II conversion regime. In this regime particle mass conversion rates are limited by the combined effects of chemical reaction and pore diffusion. Due to the reactant concentration gradients established inside particles and the associated distribution of rates of mass loss due to chemical reaction, particle diameters, apparent densities, and specific surface areas vary with mass loss when conversion is in this regime.

The aim of this work is to describe how α varies with conversion and in effect, describe how the radius and apparent density of a char particle change with conversion. Unlike other models, *e.g.*, [1,4,5], the proposed model contains no free parameters, making it more predictive. One should keep in mind, however, that the model was derived assuming ash free particles, high thermal conductivities (such that there are no temperature gradients inside the particles), and Thiele's approach to concentration gradients (which assumed first order heterogeneous kinetics). Therefore, some conclusions may not apply under certain scenarios.

Our model is concerned with the carbonaceous portion of porous char particles but it also applies to an ash-containing particle. Here ash is assumed to be uniformly distributed inside the particle, and is assumed to have no effect on reaction rates or particle temperatures. At any time, the particle apparent density is assumed to consist of the apparent density of the ash plus the apparent density of the carbonaceous portion. The apparent density of the ash is assumed to be constant while the apparent density of the carbonaceous portion of the particle is assumed to vary with mass loss, as described in this paper. Thus, carrying out the calculations on an ash-free basis (i.e., not considering the ash) and then adding in the consequences of the ash at the end of the calculation should yield the correct results for the ash-containing particle. Of course this assumes that the ash has no impact on the reactivity of the carbonaceous particle material.

2. Initial stages of char conversion

In this section, consideration is given to the initial stages of mass conversion when the particle radius, and consequently also the particle volume, is constant. Here it is assumed that for the conditions of interest (temperature, pressure, internal particle surface area, etc.), the mass consumption rate at the external surface is small compared to the mass consumption rate on internal surfaces such that the mass conversion due to the external surface can be neglected (see Appendix C for justification). Initially the particle radius will therefore stay constant for a time τ until the apparent density of a thin shell at the particle periphery has reached zero.

In the spirit of Thiele [8], the effectiveness factor is defined as

$$\eta = \frac{\text{Actual overall particle consumption rate}}{\text{Maximum overall particle consumption rate}} = \frac{\left(\frac{dm_p}{dt}\right)}{\left(\frac{dm_p}{dt}\right)_{\max}}, \tag{6}$$

where m_p is the mass of the particle. In the following, a mass consumption rate per unit volume, $R(r,t)$, will be used such that the change of mass in a thin, spherical shell with radius r and volume $dV(r,t)(=4\pi r^2 dr)$ is

$$\frac{dm(r,t)}{dt} = -R(r,t)dV(r,t). \tag{7}$$

Since $R(r,t)$ is assumed to be at its maximum at the particle surface where the reactive gas concentration is the highest *i.e.*, at $r = r_p$, the maximum possible mass conversion rate of the particle is given by

$$\left(\frac{dm_p}{dt}\right)_{\max} = -V_p R(r_p,t), \tag{8}$$

where r_p is the particle radius and $V_p = 4/3\pi r_p^3$ is the particle volume. Eqs. (6) and (8) can be combined to reveal that

$$\frac{dm_p}{dt} = \eta(t)\left(\frac{dm_p}{dt}\right)_{\max} = -\eta(t)V_p R(r_p,t), \tag{9}$$

where $\eta(t)$ is the value of the effectiveness factor at time t during the course of char conversion. In terms of char conversion x ($=1 - m_p/m_{p,0}$), the above equation can be written as

$$\frac{dx(t)}{dt} = \eta(t)V_p R(r_p,t)/m_{p,0} = \eta(t)\frac{R(r_p,t)}{\rho_{p,0}}. \tag{10}$$

This equation gives the char conversion rate at any time in terms of the reaction rate at the outer surface of the particle and the effectiveness factor at the time of interest, and the initial apparent density of the particle, $\rho_{p,0}$.

A relationship for the change in apparent density within a concentric spherical shell of radius r at any given time is obtained by dividing Eq. (7) by $dV(r,t)$: Thus,

$$\frac{d\rho(r,t)}{dt} = -R(r,t). \tag{11}$$

Separating variables and integrating yields

$$\rho(r,t) - \rho(r,0) = -\int_0^t R(r,t')dt', \tag{12}$$

and for a spherical shell at the particle periphery,

$$\rho(r_p,t) - \rho(r_p,0) = -\int_0^t R(r_p,t')dt'. \tag{13}$$

If τ is the time that it takes for the mass in this outermost shell to be completely consumed, *i.e.* the time when $\rho(r_p,t) = 0$, then

$$\rho(r_p,0) \equiv \rho_{p,0} = \int_0^\tau R(r_p,t')dt'. \tag{14}$$

For a typical CFD simulations with Lagrangian particle tracking, τ can be easily found for each particle by integrating the mass consumption rate per unit volume at the outer surface of the particle ($R(r_p,t)$), which is readily calculable given the particle size, intrinsic reactivity and temperature and ambient conditions. In practice this is done by evaluating the integral $I_\tau = \int_0^t R(r_p,t')dt'$ at every time t of a CFD simulation. When I_τ is known it is determined whether t is smaller or greater than τ by checking whether I_τ is smaller or greater than $\rho_{p,0}$. This means that for a CFD simulation, τ is *not* an input parameter to the simulation. From Eq. (14) it is seen that the time τ only depends on $\rho(r_p,0)$ and $R(r_p,t)$, which means that τ is *independent* of physical particle parameters such as porosity and internal diffusion coefficients.

When $R(r_p,t)$ is not known, one can proceed by assuming $R(r_p,t)$ and $\eta(t)$ to be independent such that the integral of the product of the two becomes the mean value of η times the integral of $R(r_p,t)$. In terms of the mean effectiveness factor:

$$\overline{\eta}(t) = \frac{1}{t}\int_{t'=0}^{t} \eta(t')dt'. \tag{15}$$

Eq. (10) can now be integrated together with Eq. (14) from $t = 0$ to τ to yield

$$x_\tau = x(\tau) = \frac{1}{\rho_{p,0}}\int_{t=0}^{\tau} \eta(t)R(r_p,t)dt = \frac{\overline{\eta}(\tau)}{\rho_{p,0}}\int_{t=0}^{\tau} R(r_p,t)dt = \overline{\eta}(\tau). \tag{16}$$

This relation indicates that char conversion at the time when the mass in the outermost shell of the particle is completely consumed (*i.e.*, at $t = \tau$) equals the mean value of the effectiveness factor. Or, in other words, τ is considered to be the time when $x = \overline{\eta}$.

For $x < x_\tau$ the radius of the particle is constant at $r_{p,0}$, the initial particle radius, while the apparent density of the particle varies with conversion: $\rho_p = \rho_{p,0}m_p/m_{p,0} = \rho_{p,0}(1-x)$. This means that for a particle having a conversion rate that falls in the zone I conversion regime where $\eta = 1$, the particle radius will be constant throughout the conversion process. On the other hand, for a particle having a conversion rate that falls in the zone III conversion regime where η is quite small, the particle radius will start to decrease for very small values of conversion.

3. After the initial stages of char conversion

At times greater than τ, Eqs. (3) and (4) are assumed to govern the change in particle size and apparent density with conversion. It is convenient to rewrite Eq. (3) as follows:

$$\frac{\rho_p + \frac{d\rho_p}{dt}dt}{\rho_p} = \left(\frac{m_p + \frac{dm_p}{dt}dt}{m_p}\right)^{\alpha}. \tag{17}$$

After a Taylor expansion of the right hand side for small dt and algebraic rearrangement, Eq. (17) becomes

$$\frac{d\rho_p}{dt} = \alpha\frac{dm_p}{dt}\frac{\rho_p}{m_p} = \frac{dm_p}{dt}\frac{\alpha}{V_p}, \tag{18}$$

when higher order terms are neglected. In the same way, Eq. (4) can be rewritten as

$$\frac{dr_p}{dt} = \beta\frac{dm_p}{dt}\frac{r_p}{m_p} = \frac{dm_p}{dt}\frac{1-\alpha}{4\pi r_p^2\rho_p}. \tag{19}$$

Before Eqs. (18) and (19) can be used to follow size and apparent density with conversion, α must be determined.

By differentiating the relationship between mass, apparent density and volume ($m_p = V_p\rho_p$), one obtains after rearrangement

$$\frac{d\rho_p}{dt} = \frac{1}{V_p}\frac{dm_p}{dt} - \frac{\rho_p}{V_p}\frac{dV_p}{dt}. \tag{20}$$

Since $V_p = 4\pi r_p^3/3$, the rate of change in particle volume can be written as

$$\begin{aligned}\frac{dV_p}{dt} &= 4\pi r_p^2\frac{dr_p}{dt} = -4\pi r_p^2\left[\left(\frac{\partial r}{\partial \rho}\right)\left(\frac{\partial \rho}{\partial t}\right)\right]_{r=r_p} \\ &= -4\pi r_p^2\left(\frac{\partial \rho(r_p,t)}{\partial r}\right)^{-1}\left(\frac{\partial \rho(r_p,t)}{\partial t}\right),\end{aligned} \tag{21}$$

where the chain rule was used for dr_p/dt and the minus sign reflects the fact that particle volume decreases in time. An expression for $\partial\rho(r_p,t)/\partial t$ can be determined by combining Eq. (11), Eq. (8) and Eq. (6) to yield

$$\frac{d\rho(r_p,t)}{dt} = \frac{1}{\eta V_p}\frac{dm_p}{dt}. \tag{22}$$

Employing this expression in Eq. (21) results in

$$\frac{dV_p}{dt} = -4\pi r_p^2\frac{1}{\eta(t)V_p}\left(\frac{dm_p}{dt}\right)\left(\frac{\partial \rho(r_p,t)}{\partial r}\right)^{-1}. \tag{23}$$

An expression for the last partial derivative on the right hand side of this equation is derived by considering the reactive gas concentration gradient inside the particle. For a single, first-order irreversible reaction consuming the carbonaceous particle material, Thiele [8] showed that at steady state, the reactant concentration within the particle is given by

$$C(r) = \frac{C_R r_p}{r}\frac{\sinh(\phi r/r_p)}{\sinh(\phi)}, \tag{24}$$

where ϕ is the Thiele modulus, a dimensionless group that gives a relative measure of chemical reaction rates to molecular diffusion rates:

$$\phi = r_p\sqrt{\frac{R(r_p)\nu}{C_R D_{\text{eff}} M_c}}. \tag{25}$$

Here ν is the stoichiometric coefficient that relates the moles of gas consumed for each mole of carbon gasified, D_{eff} is the effective diffusivity inside the particle and $R(r_p)$ is the steady state reaction rate at the particle surface: $R(r_p) = kC_R M_c/\nu$, where k is the first order rate constant and M_c is the molar weight of carbon. For $\phi < 1$, the effectiveness factor is near unity and for $\phi > 15$ the effectiveness factor is less than 0.2, indicative of char conversion with changes in both size and apparent density.

Since both the diffusive and reactive time scales, (r_p^2/D_{eff}) and $(C_R M_c/\nu R(r_p))$, respectively, are much shorter than the time scale related to the particle mass conversion $(\rho_p/R(r_p))$, it is reasonable to approximate the char conversion process as being in quasi steady-state. Assuming quasi steady-state, Eqs. (24) and (25) become

$$C(r,t) = \frac{C_R(t) r_p(t)}{r}\frac{\sinh(\phi(t) r/r_p(t))}{\sinh(\phi(t))}, \tag{26}$$

and

$$\phi(t) = r_p(t)\sqrt{\frac{k}{D_{\text{eff}}}}. \tag{27}$$

For a first-order consumption rate, Eq. (11) can be written as

$$\frac{\partial\rho(r,t)}{\partial t} = -\frac{kC(r,t)M_c.}{\nu}. \tag{28}$$

Separating variables and integrating from $t = 0$ to t results in

$$\rho(r,t) = \rho(r,0) - \int_0^t \frac{kC(r,t)M_c}{\nu}dt = \rho_{p,0} - \frac{kM_c}{\nu r} I(r,t), \tag{29}$$

where

$$I(r,t) = \int_0^t C_R(t') r_p(t')\frac{\sinh\left(\phi(t') r/r_p(t')\right)}{\sinh(\phi(t'))}dt'. \tag{30}$$

Differentiating Eq. (29) with respect to r gives

$$\frac{\partial\rho(r,t)}{\partial r} = \frac{M_c k}{\nu r}\left[\frac{I(r,t)}{r} - \frac{\partial I(r,t)}{\partial r}\right]. \tag{31}$$

For the apparent density in a thin spherical shell at the particle periphery this equation becomes

$$\frac{\partial\rho(r_p,t)}{\partial r} = \frac{M_c k}{\nu r_p}\left[\frac{I(r_p,t)}{r_p} - \frac{\partial I(r_p,t)}{\partial r}\right]. \tag{32}$$

For $\phi > 4$, it can be shown that (see Appendix A)

$$\frac{\partial I(r_p,t)}{\partial r} = \frac{\phi(t)}{r_p(t)} I(r_p,t), \tag{33}$$

and therefore

$$\frac{\partial\rho(r_p,t)}{\partial r} = \frac{kM_c}{\nu r_p^2} I(r,t)[1-\phi(t)]. \tag{34}$$

From Eq. (29), the apparent density in the shell at the periphery of the particle is

$$\rho(r_p,t) = \rho_{p,0} - \frac{kM_c}{\nu r_p(t)} I(r_p,t), \tag{35}$$

or upon rearranging, solving for $I(r_p,t)$

$$I(r_p,t) = \frac{\nu r_p(t)}{kM_c}\left[-\rho(r_p,t) + \rho_{p,0}\right]. \tag{36}$$

At the time when the mass in the outermost shell is consumed, $\rho(r_p,t) = 0$ and

$$I(r_p,t) = \frac{\rho_{p,0}\nu r_p(t)}{kM_c}. \tag{37}$$

Employing this result in Eq. (34) yields the following expression for the apparent density gradient at the particle periphery:

$$\frac{\partial\rho(r_p,t)}{\partial r} = \frac{\rho_{p,0}}{r_p(t)}(1-\phi(t)). \tag{38}$$

For a first-order reaction consuming the reactant gas, Thiele showed that the relationship between the Thiele modulus and the effectiveness factor is given by

$$\eta = \frac{3}{\phi^2}\left[\frac{\phi}{\tanh(\phi)} - 1\right]. \tag{39}$$

Since $\tanh(\phi) \approx 1$ for $\phi > 4$ the above equation reduces to

$$\eta = \frac{3}{\phi^2}[\phi - 1], \tag{40}$$

for $\phi > 4$. With this, Eq. (38) can be written as

$$\frac{d\rho(r_p,t)}{dr} = -\frac{\rho_{p,0}}{r_p(t)}\frac{\eta(t)\phi(t)^2}{3}. \tag{41}$$

Using this in Eq. (23) yields the following expression for the temporal variation in the volume of the char particle during conversion:

$$\frac{dV_p}{dt} = \frac{1}{\rho_{p,0}}\frac{dm_p}{dt}\frac{9}{\eta^2\phi^2}. \tag{42}$$

Combining the above expression with Eq. (20) yields

$$\frac{d\rho_p}{dt} = \frac{1}{V_p}\frac{dm_p}{dt}\left(1 - \frac{9}{\eta^2(t)\phi^2(t)}\frac{\rho_p}{\rho_{p,0}}\right), \tag{43}$$

which gives the temporal variation in the apparent density of the particle in terms of the mass conversion rate.

The apparent density of the particle at any time can be determined using the following expression

$$\rho_p = \frac{m_p}{V_p} = \frac{1}{V_p}\int_{r=0}^{r_p} 4\pi r^2 \rho(r,t)\,dr, \tag{44}$$

where the mass of the particle is described by an integration over the mass in all concentric spherical shells within the particle. As shown in Appendix B, the integral on the right hand side of Eq. (44) equals $\rho_{p,0}V_p(1-\eta)$ for a first-order char consumption rate. Consequently,

$$\rho_p = \rho_{p,0}(1-\eta). \tag{45}$$

Using this expression on the right hand side of Eq. (43) results in

$$\frac{d\rho_p}{dt} = \frac{1}{V_p}\frac{dm_p}{dt}\left[1 - \frac{9(1-\eta)}{\eta^2\phi^2}\right]. \tag{46}$$

By comparing Eqs. (46) and (18), the mode of conversion parameter α is identified:

$$\alpha = 1 - \frac{9(1-\eta)}{\eta^2\phi^2}. \tag{47}$$

This equation permits the evolution of α from evaluation of the Thiele modulus and effectiveness factor. For cases with large ϕ, one can make the approximation that

$$\eta = \frac{3}{\phi^2}\left[\frac{\phi}{\tanh(\phi)} - 1\right] \approx \frac{3}{\phi}. \tag{48}$$

Combining this with Eq. (47) reveals that

$$\alpha = \eta, \tag{49}$$

which shows that after the initial stages of conversion, i.e. when the diameter is decreasing with mass loss, the mode of conversion is governed by the effectiveness factor. Although Eq. (49) strictly applies for large ϕ, as shown below, it yields reasonable accurate results also for smaller values of ϕ. Thus, during the course of conversion, our model for the mode of conversion of a porous particle is given by

$$\begin{aligned}&\text{for } t \leqslant \tau\\ &\frac{dr_p}{dt} = 0 \text{ and } \frac{d\rho_p}{dt} = \frac{dm_p}{dt}\frac{1}{V_p}\\ &\text{and for } t > \tau\\ &\frac{dr_p}{dt} = \frac{dm_p}{dt}\frac{1-\eta}{4\pi r_p^2 \rho_p} \text{ and } \frac{d\rho_p}{dt} = \frac{dm_p}{dt}\frac{\eta}{V_p}.\end{aligned} \tag{50}$$

Employing Eq. (9) to determine the mass consumption rate, these equations are used to follow the variations in char particle size and apparent density during mass conversion in the calculations presented below.

4. Comparing with simulations

Simulations of heterogeneous combustion do involve a large number of uncertainties such as the homogeneous and heterogeneous chemical mechanism, the particle pore structure, treatment of particle–fluid boundary layer together with the thermodynamical parameters of both the gas and the solid. Discussing these uncertainties is, however, beyond the scope of this work. The aim of this paper is to describe the evolution of particle radius and apparent density as a function of time by utilizing models for the gradients of gas reactants and apparent density inside the particle. In the current section the predictions of the model described in the first part of this paper are compared with results from a fully resolved simulation tool in order to assess the predictability of the model. The resolved simulation tool that is used to obtain the benchmark results is previously described in Mitchell et al. [7]. In this direct numerical simulation (DNS) code, the gradients inside the particle are resolved by discretizing the particle into a large number of thin spherical shells for which the evolution equations of gas phase concentration and apparent char density are solved. In the DNS code, a multi-step adsorption/desorption reaction mechanism was used to describe the char conversion process. The reaction mechanism, as listed in Table 1, is the same as used in Mitchell et al. [7] but the rate parameters (determined from mass loss data obtained in thermogravimetric experiments) are for the char of Wyodak coal, a sub bituminous coal from Wyoming [9]. The reaction scheme is based on the turnover concept of Haynes [10], in which the carbon atoms that desorb from the carbonaceous matrix as CO or CO_2 expose an underlying carbon atom that becomes a free carbon site, a carbon site available for adsorption of gas phase species. Hurt and Haynes [11] have shown that a distribution of desorption (or adsorption) activation energies in turnover models gives rise to reacting systems that exhibit a range of reaction orders, from fractional to unity, depending on how broad the distribution is. Our mechanism and associated parameters (with a relatively large sigma on the desorption reactions) yields near first-order behavior.

Table 1
Arrhenius parameters for the surface reactions for the char of Wyodak coal. The unit of both the activation energy E_k and the distribution width σ_k is MJ/kmol.

Nr.	Reaction	A_k	E_k	σ_k
R1a	$2C_f + O_2 \rightarrow C(O) + CO$	6.50×10^{13}	102	0
R1b	$2C_f + O_2 \rightarrow C_2(O_2)$	8.95×10^{9}	55	0
R2	$C_b + C_f + C(O) + O_2 \rightarrow C(O) + CO_2 + C_f$	1.18×10^{15}	120	0
R3	$C_b + C_f + C(O) + O_2 \rightarrow 2C(O) + CO$	3.74×10^{22}	227	0
R4	$C(O) + C_b \rightarrow CO + C_f$	1.00×10^{13}	353	36
R5	$C_b + C_2(O_2) \rightarrow 2C_f + CO_2$.	1.00×10^{13}	304	33

In our simulation, the mass consumption rate per unit volume ($R(r,t)$) is calculated via the reaction mechanism presented in Table 1. This is done via the following equation:

$$R(r,t) = \frac{M_C S_{gc} m_p}{V_p}\left(\hat{RR}_{R1a}(r) + \hat{RR}_{R2}(r) + \hat{RR}_{R3}(r) + \hat{RR}_{R4}(r) + \hat{RR}_{R5}(r)\right), \tag{51}$$

where M_c is the molecular weight of carbon, S_{gc} is the specific surface area of the char, which varies with conversion according to Bhatia and Perlmutter's Random Pore Model [6], and $\hat{RR}_i$ are the reaction rates, expressed in units of moles per m^2 per second and calculated assuming an Arrhenius form for the reaction rate coefficient, as follows:

$$\hat{RR}_i(r) = A_i \exp\left(\frac{-E_i}{RT}\right)\prod [C_j(r)]^{\nu_j}. \tag{52}$$

In Eq. (52), A_i and E_i are the Arrhenius pre-factor and activation energy, respectively, and $C_j(r)$ is the concentration at that radial location r for each reactant j present in reaction i (mol/m^3 for gaseous reactants, and mol/m^2 for surface reactants) and ν_j is the stoichiometric coefficient for species j in reaction i.

Using resolved numerical simulations to check the model results instead of comparing with experimental results has the advantage that it screens out issues related to the uncertainties mentioned in the beginning of this section. Any differences between the model and the benchmark results would be due to shortcomings of the presented model in predicting particle radius and apparent density evolution. It is important to realize that for the current model there are no free parameters such that a similarity between the model and the benchmark simulations is *not* due to parameter tuning but rather shows the predictive capabilities of the model.

Three cases at different temperatures, but which all represent combustion of a 100 μm diameter char particles in an atmosphere of 6% O_2, have been simulated. The results are presented in Figs. 1 and 2. The benchmark results for the particle radius and apparent density as a function of time, obtained by the DNS code described in Mitchell et al. [7], are shown as the red lines in the two figures. The results obtained using Eq. (14) or Eq. (16) for τ are shown as the dashed black and green lines, respectively. Note that the mean effectiveness factor varies with conversion at each temperature, indicative of conversion in the zone II regime. At 1000 K, $\overline{\eta}_{\min}$ is about 0.4, and for a first-order reaction $\phi \approx 0.6$. At 1100 K, $\overline{\eta}_{\min} \approx 0.1$ and $\phi = 30$. The Thiele modulus is even greater at 1200 K.

By inspecting Fig. 1, it is noted that the time τ when the particle radius start to decrease is accurately described by Eq. (14) (black dashed line) for all three temperatures. When Eq. (16) is used to determine τ (green dashed-dotted line), the predictions are good at the two highest temperatures but not as good at the lower temperature. This is due to the fact that in obtaining Eq. (16) we made the assumption that the reactivity at the outer shell of the particle and the effectiveness factor were independent. Eq. 25 indicates that the Thiele modulus is related to the reactivity at the outer surface such that if η and ϕ are independent then also η and $R(r_p,t)$ are independent. In Fig. 3 the effectiveness factor is plotted as a function of the Thiele modulus, employing Eq. (39). As can be seen for small values of the Thiele modulus, η is strongly dependent on ϕ and hence also on $R(r_p,t)$. For larger values of the Thiele modulus, the dependence is rather weak. This explains why Eq. (16) yields good predictions for high temperatures, where the Thiele modulus

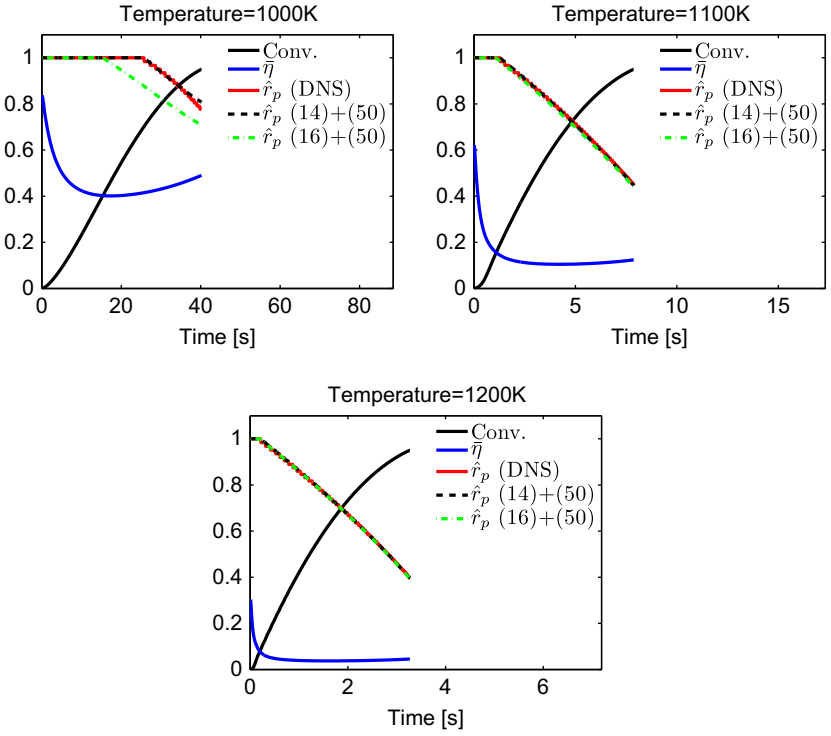

Fig. 1. Time evolution of overall conversion (black line), mean effectiveness factor (blue line) and normalized particle radius ($\hat{r}_p = r_p/r_{p,0}$) (red line) from fully resolved simulations. Also shown is the normalized particle radius obtained by using Eq. (50) when τ has been found from Eq. (14) (black dashed line) and from Eq. (16) (green dashed-dotted line). The three different panels show results from simulation with temperatures of 1000 K, 1100 K and 1200 K for 100 μm char particles exposed to 6% O_2.

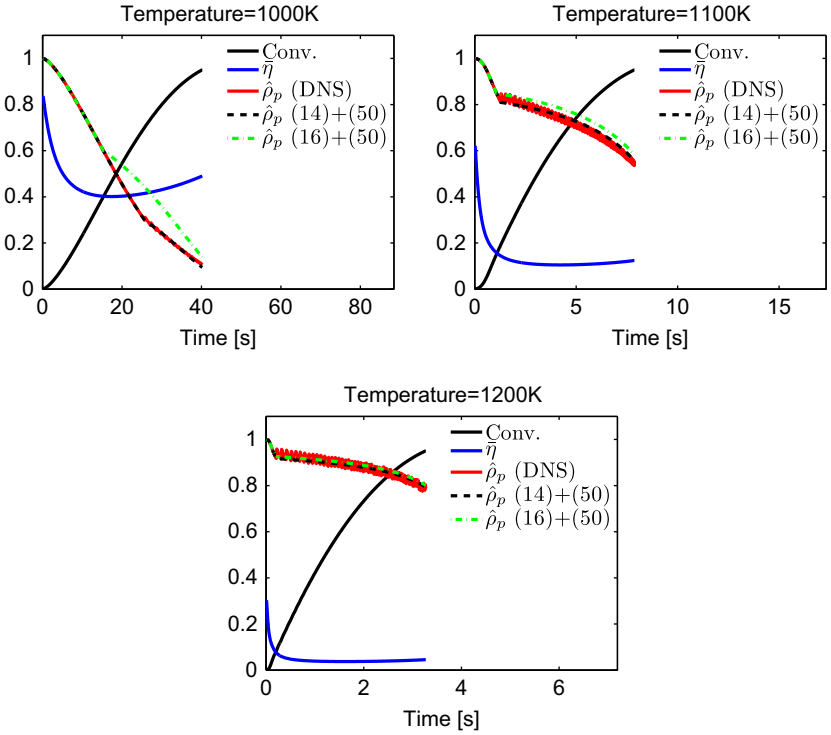

Fig. 2. Time evolution of overall conversion (black line), mean effectiveness factor (blue line) and normalized apparent density ($\hat{\rho}_p = \rho_p/\rho_{p,0}$) (red line) from fully resolved simulations. Also shown is the normalized apparent density obtained by using Eq. (50) when τ has been found from Eq. (14) (black dashed line) and from Eq. (16) (green dashed-dotted line). The three different panels show results from simulation with temperatures of 1000 K, 1100 K and 1200 K for 100 μm char particles exposed to 6% O_2.

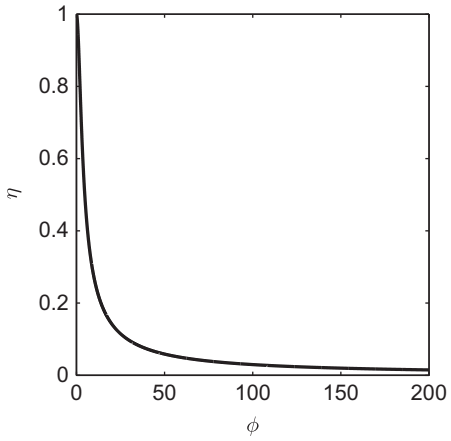

Fig. 3. Effectiveness as a function of Thiele modulus as found from Eq. (39).

is large, while the predictions are poor for the lowest temperatures where the Thiele modulus is small.

For $t > \tau$, it is seen from Figs. 1 and 2 that in particular for the two highest temperatures the model results are quiet good. For the lowest temperature the model yields results that deviate from the DNS calculations at late times. This discrepancy is a consequence of an inadequate assumption. In deriving Eq. (50), the Thiele modulus is assumed to be large (at least greater than 4), whereas at 1000 K $\phi \approx 0.6$. Despite this deviation the predictability of the model is overall found to be remarkably good.

5. Summary

A mode of conversion model relating the evolution of particle radius, apparent density and mass is presented. The model yields a time when the particle radius starts to decrease and the rates at which the radius and apparent density decrease after this time. The model itself does not include any tunable parameters. It should be kept in mind that the model presented is for an ash-free particle with uniform temperature. The apparent density of the ash-containing particle is readily calculable from the apparent density of the ash (assumed to be constant), the apparent density of the carbonaceous portion of the particle (as described by the burning mode relations) and the mass fraction of ash in the particle (as determined from $m_p/m_{p,0}$ and the mass fraction of ash in the initial char).

The time when the particle radius starts to decrease can be identified when the reactivity at the particle surface is known. If the surface reactivity is not known, however, the assumption that the surface reactivity is constant during the initial stages is made. From this it is shown that when the conversion equals the mean effectiveness factor, the particle radius will start to decrease.

After the initial stages, i.e. when the particle radius is decreasing, the model takes the approach of Thiele when describing the effects of non-uniform concentration gradients inside the particle. Here it is shown that the temporal evolution of the particle radius and the apparent density are functions of the particle mass conversion rate, the particle radius and the effectiveness factor. In addition the particle radius evolution also depends on the apparent density.

When comparing the model results with results from a fully resolved particle simulation, the model is shown to perform very well. Although it can only be shown that $\alpha = \eta$ theoretically for an irreversible first-order reaction consuming the carbonaceous particle material, we believe that the use of $\alpha = \eta$ (for use in the power-law mode of conversion expressions given by Eq. (3)) will yield calculated size and apparent density variation with mass loss that adequately agree with measurements for any choice of reaction mechanism used to describe experimental data. Based on this we claim that the current model is ideal as a sub-model for the mode of conversion of reactive porous char particles in numerical simulations.

Acknowledgments

This work forms part of the CAMPS project supported by the Research Council of Norway (215707). The work has additionally been produced with support from the BIGCCS Centre, performed under the Norwegian research program Centres for Environment-friendly Energy Research (FME). The authors acknowledge the following partners for their contributions: Aker Solutions, ConocoPhillips, Gassco, Shell, Statoil, TOTAL, GDF SUEZ and the Research Council of Norway (193816/S60).

M.B.T. acknowledges the United States Department of Energy under Award No. DE-FC26-10FE0005372.

Appendix A. The density gradient at the particle surface

To find the density gradient at the particle surface one must first find an expression for the $dI(r,t)/dr$ term in Eq. (31). From Eq. (30) we know that

$$I(r,t) = \int_0^t C_R(t') r_p(t') \frac{\sinh\left(\phi(t') r / r_p(t')\right)}{\sinh(\phi(t'))} dt', \tag{53}$$

which can be differentiated with respect to the radius to find

$$\frac{\partial I(r,t)}{\partial r} = \int_0^t \frac{\phi(t')}{r_p(t')} \frac{1}{\tanh\left(\phi(t') r / r_p(t')\right)} C_R(t') r_p(t') \times \frac{\sinh\left(\phi(t') r / r_p(t')\right)}{\sinh(\phi(t'))} dt'. \tag{54}$$

From Eq. (27) one can see that $\phi(t')/r_p(t')$ is independent of time as long as the ratio k/D_{eff} is constant. Furthermore, since $\tanh(y) \approx 1$ for $y \geqslant 4$ it is true that $\tanh\left(\phi(t') r / r_p(t')\right) \approx 1$ if $\phi(t') > 4$ since $r/r_p(t) \leqslant 1$. From this Eq. (54) can be simplified to

$$\frac{\partial I(r,t)}{\partial r} = \frac{\phi(t)}{r_p(t)} I(r,t). \tag{55}$$

Appendix B. Derivation of the particle mass

The mass of the particle at time t is found by integrating Eq. (29) over all r;

$$m_p(t) = \int_0^{r_p} 4\pi r^2 \rho(r,t) dr = \int_0^{r_p} 4\pi r^2 \left(\rho_{p,0} - \frac{k M_c}{r v} I(r,t)\right) dr = V_p(t) \rho_{p,0} - \frac{4\pi k M_c}{v} \int_0^{r_p} r I(r,t)\, dr. \tag{56}$$

In order to evaluate the integral on the right hand side, consider the following. For $\phi > 4$, Eq. (55) can be used to show that

$$\frac{d}{dr}\left(\frac{r_p(t)}{\phi(t)} I(r,t)\right) = I(r,t). \tag{57}$$

Integrating by parts yields

$$\int_0^{r_p} r I(r,t) dr = \frac{r_p^2(t)}{\phi^2(t)} I(r_p,t)(\phi(t) - 1). \tag{58}$$

Now, employing Eq. (58) in Eq. (56) yields the following for the mass of the particle in light of Eq. (37)

$$m_p(t) = V_p(t)\rho_{p,0} - \frac{4\pi\rho_{p,0}r_p^3(t)}{\phi^2(t)}(\phi(t)-1). \quad (59)$$

Using Eq. (40) now yields

$$m_p(t) = V_p\rho_{p,0}(1-\eta(t)). \quad (60)$$

Appendix C. External surface area

In a char particle there will typically by mass conversion due to both the internal surfaces, revealed through the internal pores, and due to the external surface. The external surface has an area $A_{ext} = 4\pi r_p^2$ where r_p is the radius of the char particle while the total internal surface area of the particle is given by $S_{gc}m_p$ where m_p is the mass of the char particle and S_{gc} is the specific surface area of the char. The transport of species inside the particle is diffusion controlled, and for typical char particles it is even controlled by the rather slow Knudsen diffusion. For particles with higher reactivities the entire internal surface area of the particle will therefore not be reacting. It is convenient to define the effective internal surface area based on the effectiveness factor such that

$$A_{int,eff} = S_{gc}m\eta. \quad (61)$$

When using typical values for a char of $S_{gc} = 3\times10^5$ m^2/kg, $\rho_p = 10^3$ kg/m^3 and $r_p = 10^{-4}$ m this yields

$$\frac{A_{ext}}{A_{int,eff}} = \frac{4\pi r_p^2}{S_{gc}\eta\frac{4}{3}\pi r_p^3\rho_p} = \frac{3}{r_p\rho_p S_{gc}\eta} = \frac{10^{-4}}{\eta}, \quad (62)$$

where $4\pi r_p^3/3$ was used for the mass of the particle. The above shows that for a typical char particle the external surface area is much smaller than the effective internal surface area, unless the effectiveness factor is very small. In our approach, we therefore neglect mass conversion at the external surface of the particle.

References

[1] I.W. Smith, Proc. Combust. Inst. 19 (1982) 1045–1065.
[2] R.H. Hurt, R.E. Mitchell, Proc. Combust. Inst. 24 (1992) 1233–1241.
[3] N.M. Laurendeal, Prog. Energy Combust. Sci. 4 (1978) 221.
[4] R.H. Essenhigh, Proc. Combust. Inst. 22 (1988) 89–96.
[5] R.H. Essenhigh, Combust. Flame 99 (1994) 269–279.
[6] S.K. Bhatia, D.D. Perlmutter, AIChE J. 26 (1980) 379.
[7] R.E. Mitchell, L. Ma, B.-J. Kim, Combust. Flame 151 (2007) 426.
[8] E.W. Thiele, Ind. Eng. Chem. 31 (1939) 916.
[9] R.E. Mitchell, Gasification characteristics of coal/biomass mixed fuels, DOE/NETL Quarterly Technical Progress Report No. 6, Award No. DE-FC26-10FE0005372, May 2012.
[10] B. Haynes, Combust. Flame 126 (2001) 1421–1432.
[11] R. Hurt, B. Haynes, Proc. Combust. Inst. 30 (2005) 2161–2168.